ACS APPLIED MATERIALS & INTERFACES

www.acsami.org

Research Article

Photoexcited Hot Electron Catalysis in Plasmon-Resonant Grating Structures with Platinum, Nickel, and Ruthenium Coatings

Indu Aravind, Yu Yun Wang, Yu Wang, Ruoxi Li, Zhi Cai, Bofan Zhao, Boxin Zhang, Sizhe Weng, Rifat Shahriar, and Stephen B. Cronin*

Cite This: https://doi.org/10.1021/acsami.3c16462

Read Online

ACCESS | Metrics & More | Article Recommendations | Supporting Information

ABSTRACT: We report the electrochemical potential dependence of photocatalysis produced by hot electrons in plasmon-resonant grating structures. Here, corrugated metal surfaces with a period of 520 nm are illuminated with 785 nm wavelength laser light swept as a function of incident angle. At incident angles corresponding to plasmon-resonant excitation, we observe sharp peaks in the electrochemical photocurrent and dips in the photoreflectance consistent with the conditions under which there is wavevector matching between the incident light and the spacing between the lines in the grating. In addition to the bare plasmonic metal surface (i.e., Au), which is catalytically inert, we have measured grating structures with a thin layer of Pt, Ru, and Ni catalyst coatings. For the bare Au grating, we observe that the plasmon-resonant photocurrent remains relatively featureless over the applied potential range from −0.8 to +1.2 V vs NHE. For the Pt-coated grating, we observe a sharp peak around −0.3 V vs NHE, three times larger than the bare Au grating, and near complete suppression of the oxidation half-reaction, reflecting the reducing nature of Pt as a good hydrogen evolution reaction catalyst. The photocurrent associated with the Pt-coated grating is less noisy and produces higher photocurrents than the bare Au grating due to the faster kinetics (i.e., charge transfer) associated with the Pt-coated surface. The plasmon-resonant grating structures enable us to compare plasmon-resonant excitation with that of bulk metal interband absorption simply by rotating the polarization of the light while leaving all other parameters of the experiment fixed (i.e., wavelength, potential, electrochemical solution, sample surface, etc.). A 64X plasmon-resonant enhancement (i.e., p-to-s polarized photocurrent ratio) is observed for the Pt-coated grating compared to 28X for the bare grating. The nickel-coated grating shows an increase in the hot-electron photocurrent enhancement in both oxidation and reduction half-reactions. Similarly, Ru-coated gratings show an increase in hot-electron photocurrents in the oxidation half-reaction compared to the bare Au grating. Plasmon-resonant enhancement factors of 36X and 15X are observed in the p-to-s polarized photocurrent ratio for the Ni and Ru gratings, respectively.

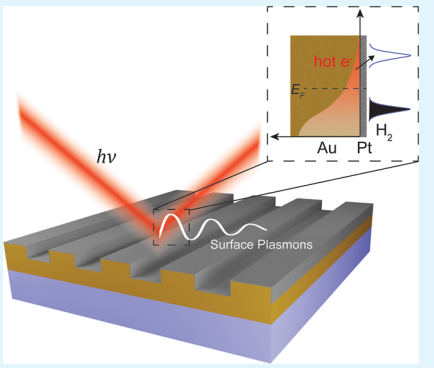

KEYWORDS: *photocatalysis, plasmonic, hot electron, water splitting, solar fuel, pt catalyst*

INTRODUCTION

The utilization of hot electrons photoexcited in plasmon-resonant nanostructures has been explored for various applications in chemistry by many research groups.[1−8] One of the great promises of hot electrons in chemistry has been to overcome high barriers and drive difficult reactions. Mukherjee et al. demonstrated H_2 dissociation through the photo-excitation of a Feshbach resonance.[9] Zhou et al. quantified the hot carrier and thermal contributions in plasmonic photocatalysis, demonstrating accelerated reaction rates and light-dependent activation barriers that outperformed heating under thermal equilibrium conditions.[10] Theoretical calculations by Sundararaman et al. and Liu et al. predicted narrow distributions of hot electrons and hot holes on early time scales (<50 ns) upon photoexcitation.[11,12] Ultrafast time-resolved spectroscopy later revealed that these photoexcited hot electrons decay rapidly into a hot Fermi distribution that persists for 1−2 ps before equilibrating with the lattice temperature.[13] Al-Zubeidi et al. showed that hot electrons generated by plasmons are injected into water to form solvated electrons and their yield is significantly increased when nanoparticle-decorated electrodes are used instead of smooth silver electrodes.[14] Angle-dependent photocurrents measured on plasmon-resonant grating structures demonstrated plasmon-resonant enhancement of photoelectrochemistry, however, the electrochemical potential dependence of these gratings has not yet been investigated.[15,16] Furthermore, no photoelectrochemical measurements have been performed on plasmon-resonant grating structures with a metal cocatalyst

Received: November 2, 2023
Revised: March 10, 2024
Accepted: March 21, 2024

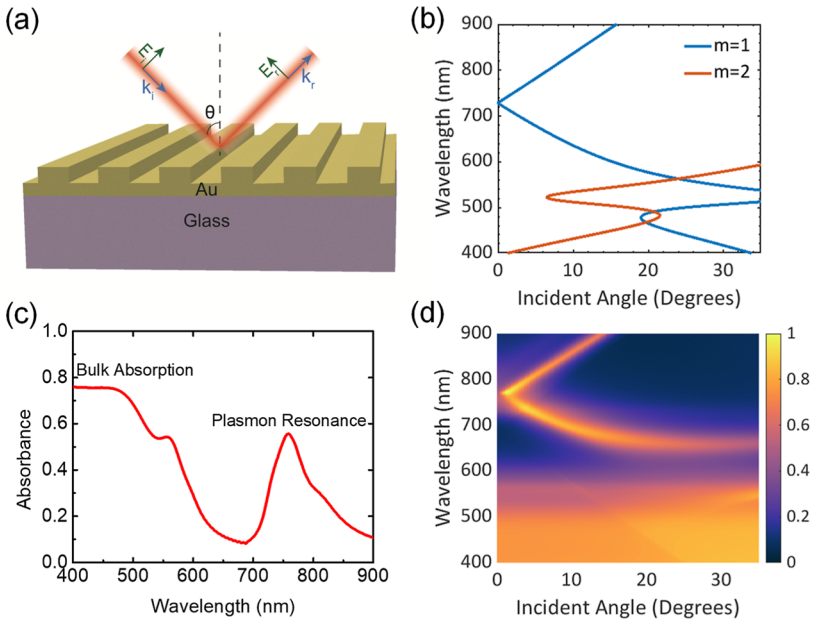

Figure 1. (a) Schematic diagram illustrating the corrugated grating structure. (b) Band structure of the Au grating calculated analytically based on diffraction conditions. (c) Simulated broadband absorption at normal incidence. (d) Absorption of Au grating simulated numerically using the FDTD method.

(e.g., Pt and Ru). Platinum (Pt)-based catalysts have been studied extensively and proven to be highly efficient for the hydrogen evolution reaction (HER).[17−19] On the other hand, ruthenium (Ru) exhibits catalytic properties that enhance the oxygen evolution reaction (OER).[20−23] Nickel (Ni) surfaces have been demonstrated to serve as good catalysts for both OER and HER.[22,24] Combining the catalytic activity of Pt, Ni, and Ru with the plasmonic properties of the metallic grating could offer an effective way to improve the efficiency of HER and OER reactions.

In the work presented here, the electrochemical potential dependence of hot electrons photoexcited in plasmon-resonant grating structures is systematically measured both with and without Pt, Ru, and Ni catalyst coatings. Conventional plasmonic metals, such as noble metals like gold (Au) and silver (Ag), possess low chemical reactivity, which constrains the types of chemical conversion that can happen on their surfaces. On the other hand, catalytic materials like Pt, Ru, and Ni have notable optical losses in the visible spectrum, leading to a weak and broadband plasmonic resonance. Nonetheless, by combining these excellent catalytic properties with those of highly plasmonic metals, it is possible to create a more efficient catalyst with multiple components. The plasmonic part can capture energy and transfer it to the catalytic component, thereby driving the desired chemical reactions. Hybrid catalytic systems offer significant potential for incorporating optical functionality, expanding the range of reactions that are only feasible with catalytic metals.[25−27] Several research groups have explored nanoparticles with plasmonic material cores and catalytic shells.[25,28−30] These studies have showcased a substantial enhancement in photocatalytic activities achieved by harnessing photons through the plasmonic core and directing the absorbed energy toward the catalytically active reaction sites located on the shell of the nanostructure.[25,27] While these structures allow precise control of the shell thickness, their optical response is polarization-independent, making it difficult to separate the plasmonic excitation from the bulk metal absorption. Grating structures make it simple to compare photocatalysis generated both on and off plasmon resonance by merely altering the polarization of the incoming light while keeping all other aspects of the reaction constant (including photon energy, sample, and electrolyte), and thus obtaining the plasmonic enhancement factor.

RESULTS AND DISCUSSION

We have designed a gold grating that supports surface plasmon resonance in the VIS-NIR range. To excite the surface plasmon polaritons (SPPs) in the grating structure, the momentum and energy of the incident photons must match that of the SPPs (i.e., wavevector matching).[15,31] Figure 1a shows a schematic diagram of the grating structure. The grating has a periodicity of 520 nm and a line width of 233 nm. The grating is on a glass substrate with 50 nm Au film and 50 nm thick Au lines. Figure 1b shows the first- and second-order surface plasmon modes of the grating, analytically calculated by solving the plasmon wavevector matching condition, with water as the surrounding medium (n = 1.328). The plasmonic mode is excited at an oblique angle with respect to normal incidence at a wavelength of 785 nm. The resonant excitation leads to enhanced absorption in the structure as verified using electromagnetic simulations. Figure 1c shows the broadband absorption spectrum of the grating at normal incidence. The first-order plasmon mode appears as a peak in absorption in the visible part of the spectrum. The second-order plasmon mode is buried within the interband absorption and appears flat in the absorption spectra at lower wavelengths. The absorption as a function of the angle and wavelength of excitation is simulated and is shown in Figure 1d (the colormap shows normalized absorption). A commercial finite-difference time-domain (FDTD) solver (Ansys Lumerical FDTD solutions) is used to solve Maxwell's equations in discrete time and space for the grating geometries. For broadband simulations at a fixed incident angle, the Broadband Fixed Angle Source Technique is used within Lumerical FDTD solutions. A power monitor is

https://doi.org/10.1021/acsami.3c16462
ACS Appl. Mater. Interfaces XXXX, XXX, XXX−XXX

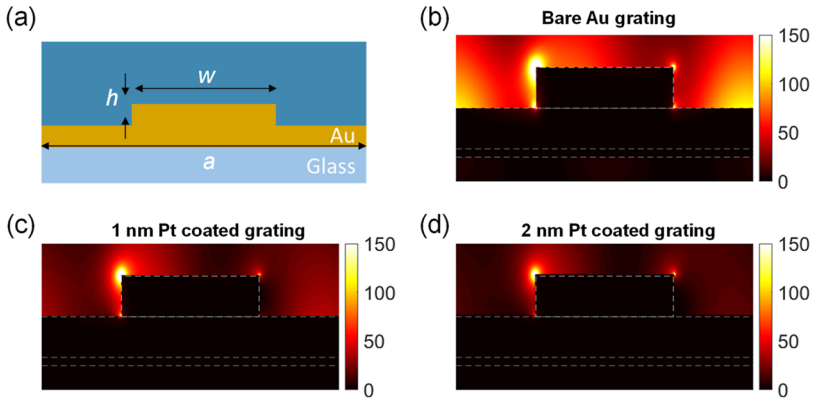

Figure 2. (a) Cross-sectional diagram of the unit cell of the corrugated grating structure. (b) Electric field enhancement of bare Au grating illuminated on resonance (angle, polarization, and wavelength). Electric field enhancement of the same Au grating with (c) 1 nm Pt and (d) 2 nm Pt coatings.

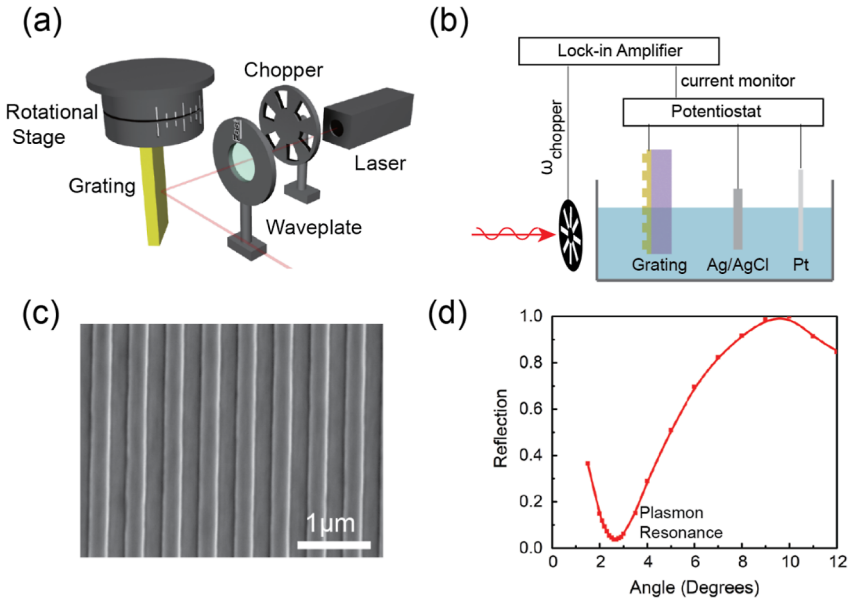

Figure 3. (a) Optical setup of the angle-dependent photocurrent measurement. (b) Electrochemical setup illustrating the AC photocurrent measurement. (c) SEM image of a Au grating with 520 nm period and 233 nm metal line width. (d) Measured photoreflection spectrum from a bare gold grating.

placed behind the source to record the reflected power (P_{ref}). Absorbed power (P_{abs}) is calculated as $P_{abs} = 1 - P_{ref}$. The resonant-enhanced absorption traces the plasmon mode expected from the analytical calculations in Figure 1b.

To investigate the effect of the thin catalytic film on the surface plasmon modes, we calculated the resonant field profiles of the Au grating structures with different thicknesses of Pt surface coatings using FDTD simulations. The electric field intensity is monitored with a 2D field monitor. Bloch boundaries are used along the *x*-direction (parallel to the grating) and perfectly matched layer boundaries are used in the *y*-direction (perpendicular to the grating) for the field calculations. A fine mesh of 0.2 nm × 0.2 nm is used in the simulations. The field enhancement at 785 nm for the bare Au grating as well as the Pt-coated gratings is plotted in Figure 2a, which shows that the field enhancement goes down as the thickness of Pt coating increases. This damping/screening of the plasmon resonance by the thicker Pt layer poses a trade-off between the hot electron generation in the Au nanostructure and the catalytic activity of the Pt coating. Both theoretically and experimentally, we find that the platinum catalyst thickness is optimized for a thickness of 1 nm. Pt films thicker than this spoil the plasmon resonance and thinner than this do not provide any significant catalytic benefit.

Figure 3a shows a schematic diagram of the experimental setup in which linearly polarized laser light is used to illuminate the plasmon-resonant grating structure mounted on a rotational stage, enabling hot electron-generated photocurrents to be measured as a function of incident angle in a pH = 7, 0.5 M Na_2SO_4 solution. The polarization of the incident light is switched between p-polarization (i.e., perpendicular to the grating lines) and s-polarization (i.e., parallel to the grating lines) using a half-wave plate. In order to detect the relatively small photocurrents generated by the short-lived hot electrons/holes, we modulate the laser using an optical chopper wheel and measure the AC photocurrent using a lock-in amplifier (Stanford Research Systems, model SR830), as illustrated in Figure 3b. The photocurrent measurements are carried out using a three-terminal potentiostat (Gamry Inc.). The differential AC lock-in technique can measure the

https://doi.org/10.1021/acsami.3c16462
ACS Appl. Mater. Interfaces XXXX, XXX, XXX−XXX

relatively small photocurrents associated with the short-lived hot electrons. The plasmon-resonant gratings are fabricated using photolithography and reactive ion etching at the University of California Santa Barbara nanofabrication facility. Figure 3c shows a scanning electron microscopy (SEM) image of the grating structure with a 520 nm period. The reflection from the grating is measured as a function of incident angle using a free-space power meter (Thorlabs S121C), as shown in Figures 3d and S1 of the Supporting Information. The thin Pt and Ru catalytic coatings were deposited using atomic layer deposition (ALD), and the Ni coating was carried out using sputtering deposition.

Figure 4a,b shows the angle-dependent photocurrent spectra of Au grating structures with and without a 1 nm-thick

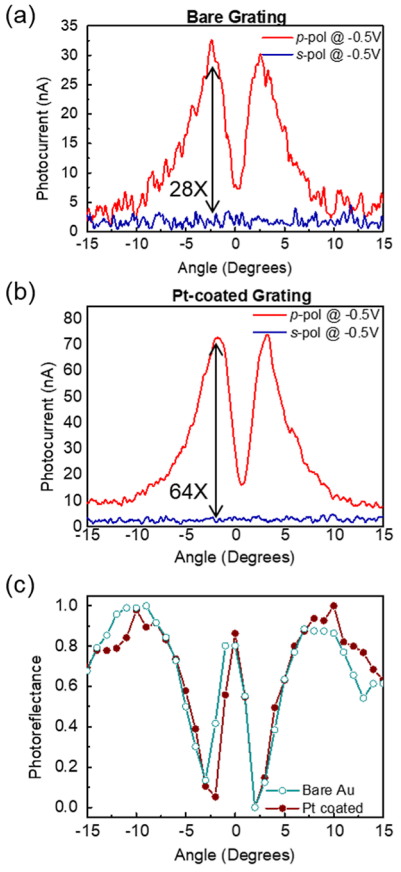

Figure 4. Angle-dependent photocurrent spectra of (a) bare gold and (b) Pt-coated gold grating nanostructures. (c) Normalized photoreflectance spectra taken with and without the platinum coating.

platinum coating. Spectra are plotted for both s-polarized (nonresonant) and p-polarized (resonant) light at an applied potential of −0.5 V vs Ag/AgCl. Here, sharp peaks can be seen in the AC photocurrent at ±2.3° (from normal incidence) for p-polarized light. However, s-polarized light shows no angle dependence and substantially lower photocurrents. The plasmon resonance in our grating system is polarization-dependent, which enables us to isolate the plasmon-generated photocurrent from other sources. When the polarization is tuned to the s-polarization, the excitation is nonresonant, and there will not be any plasmon-mediated photocurrent. On the other hand, when the excitation is tuned to the p-polarization with respect to the grating plane, there will be plasmon-generated hot electron-mediated photocurrent, which gets modulated at the chopping frequency of the laser. The AC photocurrent can thereby be isolated using the sensitive lock-in measurement technique. This sort of distinction is characteristic of the polarization-sensitive system and the measurement technique. Here, based on the p-to-s polarized photocurrent ratio, we establish that the plasmon-resonant enhancement factor is 28X for the bare Au grating (Figure 4a) and 64X for the Pt-coated Au grating (Figure 4b). In addition, the photocurrent associated with the Pt-coated grating is less noisy and produces higher photocurrents than the bare Au grating due to the faster kinetics (i.e., charge transfer) associated with the Pt-coated surface. The peaks in the photocurrent coincide nicely with the peaks observed in the photoreflectance spectra plotted in Figure 4c.

We have conducted similar experiments on Au gratings coated with Ru and Ni thin films, measuring photocurrent as a function of incident angle, polarization, and electrochemical potential. Figure 5a,c shows the angle-dependent photocurrent measured at +1.4 V vs Ag/AgCl using Ni and Ru-coated gratings, respectively. Figure 5b,d shows the angle-dependent photoreflection from these gratings compared to that of the corresponding bare Au grating. The dips in photoreflection correspond to the plasmon excitation and are relatively undisturbed due to the presence of the surface coatings. The Ni-coated and Ru-coated gratings show plasmon-resonant enhancement factors (i.e., p-to-s polarized photocurrent ratio) of 36X and 15X, respectively, at +1.4 V.

The plasmonic field enhancement of bare Au gratings diminishes in the presence of even a very thin layer (1 nm) of surface coating as evident from the electromagnetic simulations (Figure 2). Nevertheless, the Au gratings with these catalytic metal coatings show enhanced photocurrent compared to the bare grating. The plasmonic nearfield is strongly confined to a very small mode volume around the Au grating. Here, the photochemical reactions occur mostly by the transfer of hot carriers to the molecular adsorbates at the interfacial barrier between metal and adsorbate. During photocatalysis, when molecules interact with the metal surface, the narrower d-band of the metal hybridizes the molecular orbital into metal−adsorbate bonding and antibonding modes. In the case of bare Au gratings, the antibonding mode can be below the Fermi level due to the deep-lying d band of the Au. As a result, the molecule is less likely to adsorb onto the Au surface, thereby limiting the transfer of plasmon-generated hot electrons. On the other hand, when catalytic metals such as Pt and Ru interact with adsorbates, generally only the bonding states are below the Fermi level, leading to chemisorption.[27] The increased number density of hybridized surface states between metal and adsorbates increases the dephasing channels for the plasmons, thus, overcoming the reduction in hot electron generation rate.

The sensitivity of plasmon-mediated photocatalysis to the surface-bound species makes it an attractive tool to study the metal-molecular electrochemical interactions. Figure 6 shows the electrochemical potential dependence of the AC photocurrent produced by illuminating the bare Au gratings and catalyst-coated gratings on resonance (i.e., *p*-polarized light at approximately θ = 2.3°) from −0.8 to +1.2 V versus NHE. Figure 6a shows the potential-dependent photocurrent produced with a bare Au grating. The photocurrent increases monotonically as the potential is reduced to −0.4 V and then saturates. On the oxidation side, the photocurrent is relatively low compared to the reduction side. Overall, the potential-

https://doi.org/10.1021/acsami.3c16462
ACS Appl. Mater. Interfaces XXXX, XXX, XXX−XXX

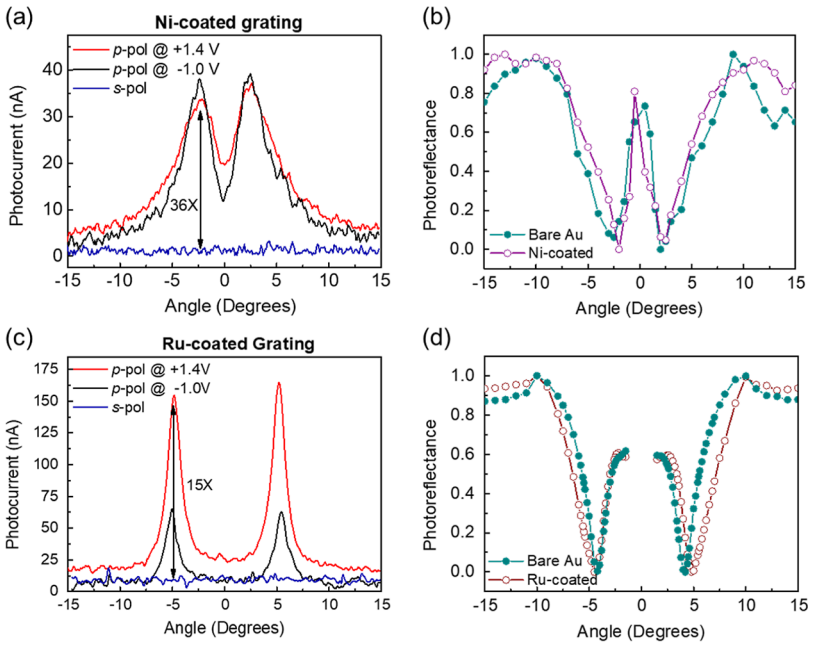

Figure 5. (a) Angle-dependent photocurrent spectra of Ni-coated gold grating nanostructure. (b) Photoreflectance spectra with and without nickel coating. (c) Angle-dependent photocurrent spectra of Ru-coated gold grating nanostructure. (d) Photoreflectance spectra with and without ruthenium coating.

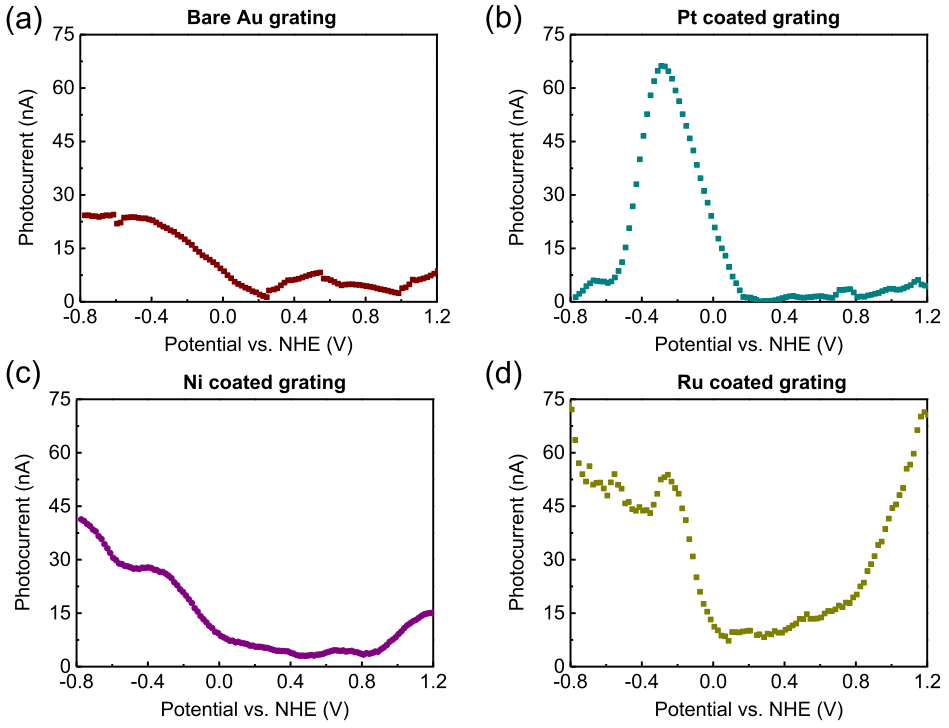

Figure 6. (a) Electrochemical potential dependence of the AC photocurrent measured on resonance with a gold grating structure (a) bare, (b) Pt coating, (c) Ni coating, and (d) Ru coating.

dependent photocurrent in the bare Au grating is relatively featureless, reflecting the poor catalytic properties of the Au surface. In Figure 6b, however, we observe a clear resonant feature centered around −0.3 V versus NHE for the Pt-coated gratings. This corresponds to the conditions under which the energy of the hot electrons photoexcited in the gold passes through a resonance with the prevailing/dominant redox potential in solution and/or reactant species bound to the catalyst surface. This resonant feature is observed repeatedly over many different cycles (i.e., potential sweeps) and different samples, as plotted in Figure S8 of the Supporting Information document. The fact that there is no corresponding peak observed under oxidizing potentials reflects the reducing nature of the platinum catalyst surface, which favors HER over OER.[8,32,33] In addition, the peak photocurrent measured on the Pt-coated grating is roughly 2.3X higher than that of the

https://doi.org/10.1021/acsami.3c16462
ACS Appl. Mater. Interfaces XXXX, XXX, XXX−XXX

bare Au grating. The nickel-coated grating (Figure 6c) shows an increase in the hot-electron photocurrent compared to bare Au grating both above +0.8 V and below −0.6 V vs NHE, indicating slight catalytic enhancement in both oxidation and reduction half-reactions. Similarly, the Ru-coated grating (Figure 6d) shows an increase in hot-electron photocurrent above +0.8 V and below 0 V vs NHE. Compared to bare Au grating, the photocurrent increases rapidly with potential on both the reduction and oxidation sides for the Ru-coated grating. On the reduction side, the rate of increase of photocurrent for the Ru-coated grating is similar to that of the Pt-coated grating until the potential reaches −0.4 V. Below this potential, the photocurrent for the Ru-coated grating rises steadily. These data show that the hot electron-driven photocurrent is quite sensitive to the catalyst surface composition and the electrochemical potential, both of which affect the surface-bound intermediates, which thereby increase/decrease the charge transfer rates of these short-lived hot electrons.

This photoelectrochemical approach provides energetic spectroscopy of surface-bound intermediate species. While there are many functional groups on the photoelectrode surface such as OH, OOH, and H, for large negative potentials, we expect the dominant reduction half-reaction to be HER. For high positive potentials, we expect the dominant half-reaction to be OER. In the intermediate range, it is unclear which surface intermediates are dominating these AC photocurrent spectra. That is, for potentials below −0.4 V vs NHE, we believe the AC photocurrent is largely due to surface-bound H^+ ions, and for potentials above +0.8 V vs NHE (for Ru and Ni), the AC photocurrent is largely due to surface-bound OH^- ions. Nevertheless, we observe characteristically distinct voltage sweeps (i.e., spectra) for different catalytic surfaces (i.e., Pt, Ru, Au, and Ni). For example, the peak-like nature of the features observed on Pt and Ru between −0.3 and −0.4 V could be due to the electrochemical desorption of surface species. That is, sweeping the potential through the resonant energy results in an increase and then a drop in the AC photocurrent, as these species are depleted. Future studies will be needed in order to unambiguously identify these surface species possibly by varying the electrolyte composition and/or scan rate.

CONCLUSIONS

In conclusion, we have demonstrated a differential AC spectroscopy approach that provides a very sensitive way to measure surface species/catalyst surface interactions as a function of electrode potential. We observe that the ultrathin catalyst coatings (∼1 nm thick) do not affect the plasmon-enhanced hot electron generation in Au gratings. These catalytic coatings enhance the charge transfer rates associated with these short-lived hot electrons involved in hydrogen evolution and OERs. Due to the plasmon resonance excitation of hot electrons, a 64X enhancement in the ratio of p-to-s polarization ratio is observed for the Pt-coated grating, and a 28X enhancement is observed for the bare Au grating. Ni-coated and Ru-coated gratings show an enhancement in the plasmon-resonant photocurrent under both oxidative and reducing potentials compared to the bare Au grating. The catalytic surface coatings significantly alter the interaction of adsorbate molecules with the grating surface, and the potential-dependent photocurrent traces show distinctive behavior corresponding to the electronic interaction of the molecule/metal complex at this interface.

EXPERIMENTAL SECTION

Fabrication. A 5 nm thick Ti film followed by a 100 nm thick gold film was deposited onto a transparent BK-7 substrate. The grating lines were patterned onto the gold film using an ASML deep UV stepper lithography tool and by partially etching the film to a depth of 50 nm. 1 nm Pt and Ru depositions were carried out using ALD at 200 °C with 31 cycles and 270 °C with 26 cycles, respectively. The precursors used were $(MeCp)PtMe_3$ and oxygen gas for Pt and Ru(EtCp) and oxygen gas for Ru. The partial pressure of oxygen inside the chamber was around 1.5 Torr.[19] The Ni-coated grating samples were fabricated by sputter depositing Ni metal using an Ar plasma. To achieve 1 nm thick Ni, deposition was carried out for 8 s with a deposition rate of 1.3 Å/s. A copper wire was attached to the grating for electrical contact using silver paint (SPI Supplies Inc.) and then sealed with epoxy (Devcon).

Photocurrent Measurements. The 1 cm × 1 cm grating was mounted on a motorized rotational stage (Thorlabs CR1-Z7, and KDC101) and immersed in a 0.5 M Na_2SO_4 aqueous solution. A linearly polarized free space laser (Oxxius L4Cc) at 785 nm wavelength was used to illuminate the center of the grating structure. The beam diameter was approximately 2 mm, and the optical power illuminating the grating was around 10 mW. The incident angle was changed by rotating the grating with respect to the beam. A half-wave plate was inserted in the beam path to rotate the incident polarization between s-polarization (resonance off) and p-polarization (resonance on). A 3-terminal Gamry potentiostat was used to measure the electrochemical current in the system with the grating as the working electrode, Ag/AgCl (3 M NaCl) as the reference electrode (BASI Inc.), and a Pt wire as the counter electrode. When the resonance was turned on, a small hot electron photocurrent was added to the electrochemical current. To isolate this photocurrent from the DC electrochemical current, the laser beam was modulated using a chopper wheel at 200 Hz frequency. The small modulation in Gamry electrochemical current at 200 Hz frequency was separated using a lock-in amplifier (Stanford Research Systems, model SR830).

ASSOCIATED CONTENT

Supporting Information

The Supporting Information is available free of charge at https://pubs.acs.org/doi/10.1021/acsami.3c16462.

Photoreflectance measurement setup, fabrication details, UV−vis spectra of bare and Pt-coated grating, Pt thickness dependence of the photocurrent enhancement, potential-dependent photocurrent, and time dependence of the potential sweeps (PDF)

AUTHOR INFORMATION

Corresponding Author

Stephen B. Cronin − *Department of Physics and Astronomy, University of Southern California, Los Angeles, California 90089, United States; Ming Hsieh Department of Electrical and Computer Engineering and Department of Chemistry, University of Southern California, Los Angeles, California 90089, United States;* orcid.org/0000-0001-9153-7687; Email: scronin@usc.edu

Authors

Indu Aravind − *Department of Physics and Astronomy, University of Southern California, Los Angeles, California 90089, United States;* orcid.org/0000-0002-0908-9887

Yu Yun Wang − *Ming Hsieh Department of Electrical and Computer Engineering, University of Southern California, Los*

https://doi.org/10.1021/acsami.3c16462
ACS Appl. Mater. Interfaces XXXX, XXX, XXX−XXX

Angeles, California 90089, United States; orcid.org/0000-0003-0620-5069

Yu Wang − *Mork Family Department of Chemical Engineering and Materials Science, University of Southern California, Los Angeles, California 90089, United States;* orcid.org/0000-0002-0307-1301

Ruoxi Li − *Mork Family Department of Chemical Engineering and Materials Science, University of Southern California, Los Angeles, California 90089, United States;* orcid.org/0000-0002-6432-6072

Zhi Cai − *Mork Family Department of Chemical Engineering and Materials Science, University of Southern California, Los Angeles, California 90089, United States;* orcid.org/0000-0002-3741-5715

Bofan Zhao − *Ming Hsieh Department of Electrical and Computer Engineering, University of Southern California, Los Angeles, California 90089, United States;* orcid.org/0000-0003-0478-6330

Boxin Zhang − *Mork Family Department of Chemical Engineering and Materials Science, University of Southern California, Los Angeles, California 90089, United States*

Sizhe Weng − *Ming Hsieh Department of Electrical and Computer Engineering, University of Southern California, Los Angeles, California 90089, United States;* orcid.org/0000-0002-6555-2442

Rifat Shahriar − *Ming Hsieh Department of Electrical and Computer Engineering, University of Southern California, Los Angeles, California 90089, United States*

Complete contact information is available at: https://pubs.acs.org/10.1021/acsami.3c16462

Notes

The authors declare no competing financial interest.

■ ACKNOWLEDGMENTS

This research was supported by the Army Research Office (ARO) award no. W911NF-22-1-0284 (I.A.); the Office of Naval Research (ONR) Award no. N000142212697 (Z.C.); the U.S. Department of Energy, Office of Basic Energy Sciences award no. DESC0019322 (R.S., R.L.); the National Science Foundation (NSF) award nos. CHE-2106480 (S.W.) and CBET-2012845 (Y.W.); and the Air Force Office of Scientific Research (AFOSR) grant no. FA9550-19-1-0115 (B.Z.). The fabrication and characterization were carried out at the University of California Santa Barbara (UCSB) Nanofabrication Facility, the University of Southern California (USC) Core Nanofabrication Facility, the USC Core Center of Excellence in Nano Imaging (CNI), and the California Nano Systems Institute, University of California Los Angeles (UCLA).

■ REFERENCES

(1) Linic, S.; Christopher, P.; Ingram, D. B. Plasmonic-Metal Nanostructures for Efficient Conversion of Solar to Chemical Energy. *Nat. Mater.* **2011**, *10*, 911−921.

(2) Christopher, P.; Xin, H.; Marimuthu, A.; Linic, S. Singular Characteristics and Unique Chemical Bond Activation Mechanisms of Photocatalytic Reactions on Plasmonic Nanostructures. *Nat. Mater.* **2012**, *11*, 1044−1050.

(3) Christopher, P.; Xin, H.; Linic, S. Visible-Light-Enhanced Catalytic Oxidation Reactions on Plasmonic Silver Nanostructures. *Nat. Mater.* **2011**, *3*, 467−472.

(4) Ghobadi, T. G. U.; Ghobadi, A.; Ozbay, E.; Karadas, F. Strategies for Plasmonic Hot-Electron-Driven Photoelectrochemical Water Splitting. *ChemPhotoChem* **2018**, *2*, 161−182.

(5) Hou, W.; Cronin, S. B. A Review of Surface Plasmon Resonance-Enhanced Photocatalysis. *Adv. Funct. Mater.* **2013**, *23*, 1612−1619.

(6) Hou, W.; Liu, Z.; Pavaskar, P.; Hung, W. H.; Cronin, S. B. Plasmonic Enhancement of Photocatalytic Decomposition of Methyl Orange under Visible Light. *J. Catal.* **2011**, *277*, 149−153.

(7) Wang, S.; Lu, A.; Zhong, C.-J. Hydrogen Production from Water Electrolysis: Role of Catalysts. *Nano Convergence* **2021**, *8*, 4.

(8) Li, C.; Baek, J.-B. Recent Advances in Noble Metal (Pt, Ru, and Ir)-Based Electrocatalysts for Efficient Hydrogen Evolution Reaction. *ACS Omega* **2020**, *5*, 31−40.

(9) Mukherjee, S.; Zhou, L.; Goodman, A. M.; Large, N.; Ayala-Orozco, C.; Zhang, Y.; Nordlander, P.; Halas, N. J. Hot-Electron-Induced Dissociation of H2 on Gold Nanoparticles Supported on Sio2. *J. Am. Chem. Soc.* **2014**, *136*, 64−67.

(10) Zhou, L.; Swearer, D. F.; Zhang, C.; Robatjazi, H.; Zhao, H.; Henderson, L.; Dong, L.; Christopher, P.; Carter, E. A.; Nordlander, P.; et al. Quantifying Hot Carrier and Thermal Contributions in Plasmonic Photocatalysis. *Science* **2018**, *362*, 69−72.

(11) Liu, J. G.; Zhang, H.; Link, S.; Nordlander, P. Relaxation of Plasmon-Induced Hot Carriers. *ACS Photonics* **2018**, *5*, 2584−2595.

(12) Sundararaman, R.; Narang, P.; Jermyn, A. S.; Goddard III, W. A., Iii; Atwater, H. A. Theoretical Predictions for Hot-Carrier Generation from Surface Plasmon Decay. *Nat. Commun.* **2014**, *5*, 5788.

(13) Wang, Y.; Shen, L.; Wang, Y.; Hou, B.; Gibson, G.; Poudel, N.; Chen, J.; Shi, H.; Guignon, E.; Cady, N. C.; Page, W. D.; et al. Hot Electron-Driven Photocatalysis and Transient Absorption Spectroscopy in Plasmon Resonant Grating Structures. *Faraday Discuss.* **2019**, *214*, 325−339.

(14) Al-Zubeidi, A.; Ostovar, B.; Carlin, C. C.; Li, B. C.; Lee, S. A.; Chiang, W.-Y.; Gross, N.; Dutta, S.; Misiura, A.; Searles, E. K.; et al. Mechanism for Plasmon-Generated Solvated Electrons. *Proc. Natl. Acad. Sci. U.S.A.* **2023**, *120*, No. e2217035120.

(15) Wang, Y.; Aravind, I.; Cai, Z.; Shen, L.; Gibson, G. N.; Chen, J.; Wang, B.; Shi, H.; Song, B.; Guignon, E.; et al. Hot Electron Driven Photocatalysis on Plasmon-Resonant Grating Nanostructures. *ACS Appl. Mater. Interfaces* **2020**, *12*, 17459−17465.

(16) Shen, L.; Gibson, G. N.; Poudel, N.; Hou, B.; Chen, J.; Shi, H.; Guignon, E.; Cady, N. C.; Page, W. D.; Pilar, A.; et al. Plasmon Resonant Amplification of Hot Electron-Driven Photocatalysis. *Appl. Phys. Lett.* **2018**, *113*, 113104.

(17) Subbaraman, R.; Tripkovic, D.; Strmcnik, D.; Chang, K.-C.; Uchimura, M.; Paulikas, A. P.; Stamenkovic, V.; Markovic, N. M. Enhancing Hydrogen Evolution Activity in Water Splitting by Tailoring Li+-Ni(Oh)2-Pt Interfaces. *Science* **2011**, *334*, 1256−1260.

(18) Yin, H.; Zhao, S.; Zhao, K.; Muqsit, A.; Tang, H.; Chang, L.; Zhao, H.; Gao, Y.; Tang, Z. Ultrathin Platinum Nanowires Grown on Single-Layered Nickel Hydroxide with High Hydrogen Evolution Activity. *Nat. Commun.* **2015**, *6*, 6430.

(19) Cheng, N.; Stambula, S.; Wang, D.; Banis, M. N.; Liu, J.; Riese, A.; Xiao, B.; Li, R.; Sham, T.-K.; Liu, L.-M.; et al. Platinum Single-Atom and Cluster Catalysis of the Hydrogen Evolution Reaction. *Nat. Commun.* **2016**, *7*, 13638.

(20) Reier, T.; Oezaslan, M.; Strasser, P. Electrocatalytic Oxygen Evolution Reaction (Oer) on Ru, Ir, and Pt Catalysts: A Comparative Study of Nanoparticles and Bulk Materials. *ACS Catal.* **2012**, *2*, 1765−1772.

(21) Cao, X.; Huo, J.; Li, L.; Qu, J.; Zhao, Y.; Chen, W.; Liu, C.; Liu, H.; Wang, G. Recent Advances in Engineered Ru-Based Electrocatalysts for the Hydrogen/Oxygen Conversion Reactions. *Adv. Energy Mater.* **2022**, *12*, 2202119.

(22) Cao, L.; Luo, Q.; Chen, J.; Wang, L.; Lin, Y.; Wang, H.; Liu, X.; Shen, X.; Zhang, W.; Liu, W.; et al. Dynamic Oxygen Adsorption on Single-Atomic Ruthenium Catalyst with High Performance for Acidic Oxygen Evolution Reaction. *Nat. Commun.* **2019**, *10*, 4849.

(23) Ying, J.; Chen, J.-B.; Xiao, Y.-X.; Cordoba de Torresi, S. I.; Ozoemena, K. I.; Yang, X.-Y. Recent Advances in Ru-Based Electrocatalysts for Oxygen Evolution Reaction. *J. Mater. Chem. A* **2023**, *11*, 1634−1650.
(24) Xiaodong, C.; Jianqiao, L.; Tiefeng, Y.; Zhiyuan, Z.; Chunyu, S.; Shuai, Y.; Xin, G.; Nannan, W.; Lifeng, C. Recent Advances in Earth-Abundant First-Row Transition Metal (Fe, Co and Ni)-Based Electrocatalysts for the Oxygen Evolution Reaction. *Energy Mater.* **2022**, *2*, 200028.
(25) Aslam, U.; Chavez, S.; Linic, S. Controlling Energy Flow in Multimetallic Nanostructures for Plasmonic Catalysis. *Energy Mater.* **2017**, *12*, 1000−1005.
(26) Aslam, U.; Rao, V. G.; Chavez, S.; Linic, S. Catalytic Conversion of Solar to Chemical Energy on Plasmonic Metal Nanostructures. *Nat. Catal.* **2018**, *1*, 656−665.
(27) Sytwu, K.; Vadai, M.; Dionne, J. A. Bimetallic Nanostructures: Combining Plasmonic and Catalytic Metals for Photocatalysis. *Adv. Phys.: X* **2019**, *4*, 1619480.
(28) Chen, D.; Li, C.; Liu, H.; Ye, F.; Yang, J. Core-Shell Au@Pd Nanoparticles with Enhanced Catalytic Activity for Oxygen Reduction Reaction Via Core-Shell Au@Ag/Pd Constructions. *Sci. Rep.* **2015**, *5*, 11949.
(29) Sun, Y.-B.; Ni, M.; Chi, C.; Yang, D.-R.; Chen, X.-L.; Qi, Q.; Li, J.; Xia, X.-H. Plasmon Driven Super-High Her Activity of Electronic Structure and Lattice Strain Engineered Single Atomic Layer Pd@Au Nanorods. *Chem. Eng. J.* **2023**, *467*, 143387.
(30) Bayles, A.; Tian, S.; Zhou, J.; Yuan, L.; Yuan, Y.; Jacobson, C. R.; Farr, C.; Zhang, M.; Swearer, D. F.; Solti, D.; et al. Al@Tio2 Core-Shell Nanoparticles for Plasmonic Photocatalysis. *ACS Nano* **2022**, *16*, 5839−5850.
(31) Aravind, I.; Wang, Y.; Cai, Z.; Shen, L.; Zhao, B.; Yang, S.; Wang, Y.; Dawlaty, J. M.; Gibson, G. N.; Guignon, E.; et al. Hot Electron Plasmon-Resonant Grating Structures for Enhanced Photochemistry: A Theoretical Study. *Crystals* **2021**, *11*, 118.
(32) Kibsgaard, J.; Chorkendorff, I. Considerations for the Scaling-up of Water Splitting Catalysts. *Nat. Energy* **2019**, *4*, 430−433.
(33) Liu, X.; Hao, Z.; Wang, H.; Wang, T.; Shen, Z.; Zhang, H.; Zhan, S.; Gong, J. Enhanced Localized Dipole of Pt-Au Single-Site Catalyst for Solar Water Splitting. *Proc. Natl. Acad. Sci. U.S.A.* **2022**, *119*, No. e2119723119.

https://doi.org/10.1021/acsami.3c16462
ACS Appl. Mater. Interfaces XXXX, XXX, XXX−XXX